Dynamical transitions of a low-dimensional model for Rayleigh-Bénard convection under a vertical magnetic field

Daozhi Han[a,b,*], Marco Hernandez[b], Quan Wang[b,c]

[a] Department of Mathematics and Statistics, Missouri University of Science and Technology, 400 W 12th St, Rolla, MO
[b] The Institute for Scientific Computing and Applied Mathematics, Indiana University, 831 East Third Street, Bloomington, IN
[c] Department of Mathematics, Sichuan University, Chengdu, Sichuan, China

Abstract

In this article, we study the dynamic transitions of a low-dimensional dynamical system for the Rayleigh-Bénard convection subject to a vertically applied magnetic field. Our analysis follows the dynamical phase transition theory for dissipative dynamical systems based on the principle of exchange of stability and the center manifold reduction. We find that, as the Rayleigh number increases, the system undergoes two successive transitions: the first one is a well-known pitchfork bifurcation, whereas the second one is structurally more complex and can be of different type depending on the system parameters. More precisely, for large magnetic field, the second transition is of continuous type and gives to a stable limit cycle; on the other hand, for low magnetic field or small height-to-width aspect ratio, a jump transition occurs where an unstable periodic orbit eventually collides with the stable steady state, leading to the loss of stability at the critical Rayleigh number. Finally, numerical results are presented to corroborate the analytic predictions.

Keywords: dynamical transitions, bifurcation, Rayleigh-Bénard convection, centre manifold reduction, dynamical system

*Corresponding author
Email addresses: handaoz@mst.edu (Daozhi Han), hernmarc@indiana.edu (Marco Hernandez), wqxihujunzi@126.com (Quan Wang)

Preprint submitted to Chaos, Solitons&Fractals *July 21, 2018*

2010 MSC: 37D45, 35Q99, 34C23

1. Introduction

The Rayleigh-Bénard (RB) convection is a classical buoyancy-driven convection problem that is relevant for the study of thermal convection phenomena in geophysical science and many engineering applications. It describes the motion of a horizontal fluid layer heated from below and cooled on the top. The dynamic behaviour of the fluid is determined by the Rayleigh number. As Rayleigh number increases, the convection state undergoes a sequence of bifurcations (transitions) leading to developed turbulence. Hence the Rayleigh-Bénard convection serves as a fundamental example for the study of nonlinear dynamics such as bifurcations, pattern formation, instabilities and turbulence [1].

The stability and bifurcation of the RB convection at the first transition is well-known, see for instance [2, 3] for the linear stability analysis, and [4, 5, 6, 7] for nonlinear theories, among many others. In particular, the authors in [7, 8] show that the Rayleigh-Bénard problem bifurcates from the basic state to an attractor when the Rayleigh number crosses the first critical Rayleigh number under physically sound boundary conditions. Recently, they have classified the solutions in the bifurcated attractor and obtained detailed structures of the solutions of the Bénard problem in physical space (rolls, rectangles, hexagons, etc.), see [9, 10] for details. Their nonlinear method is based on the geometric theory for incompressible flows [11] and the bifurcation and stability theory for nonlinear dynamical systems [12].

While the theory of the first transition for the RB convection is rather complete, there is a lack of systematic mathematical study on the second transition, partly due to the absence of explicit formulations of the bifurcated solutions. In this article, we focus on the study of the bifurcation and classification of the dynamic transition of a low-dimensional model (a system of nonlinear ordinary differential equations) for the RB convection in the presence of magnetic field–also known as hydromagnetic convection. The RB convection under the influence of magnetic field is important for a number of geophysical and astrophysical problems [2, 13]. It also has many industrial applications, such as, in crystal growth, in fusion reactor and in the manufacture of semiconductors. Because of its importance, many research based on numerical simulations and real-world experiments have been carried out to study the instabilities and bifurcations associated with hydromagnetic convection, see [14, 15, 16, 17, 18, 13, 19, 20, 21, 22, 23, 24] and references therein. These study reveals the stabilizing effect of magnetic field (Lorentz force) in RB convection by suppressing the unstable fluctuations and degenerating turbulence.

Our study on the dynamical transition of the RB convection in the presence of a vertically applied magnetic field is based on a low-dimensional dynamical system–a set of nonlinear ordinary differential equations. The system is derived by truncating a two-dimensional Boussinesq model for the RB convection in an incompressible conducting fluid in the Fourier series expansions, in the spirit of the celebrated Lorentz system [25]; see Sec. 2 for details. This simplified low-dimensional dynamical system was previously employed in [26] in the numerical investigation of the RB convection in an incompressible conducting fluid subjected to a magnetic field.

In this article, we are interested in the classification and characterization of the first and second transitions in a low-dimensional dynamical system for the RB convection with the influence of magnetic field. We follow the approach of the dynamic phase transition theory for dissipative dynamical systems [27] which is developed based on the principle of exchange of stability and the center manifold reduction. See also [28, 29, 30, 31, 32] for applications of the theory. In the study, we focus on the effect of magnetic field on the transition. We find that, in loose terms, for large magnetic field, the system undergoes a continuous transition as the Rayleigh number crosses the second critical value (a continuous sequence of limit cycles emerge), while for low magnetic field a jump transition occurs (a butterfly orbit is present through the transition). Moreover, the effect of magnetic field on the transition depends on the aspect ratio. There exists a critical aspect ratio below which only jump transition is possible no matter how strong the magnetic field is. These results confirm the stabilizing effect of magnetic field in the RB convection.

The rest of the article is organized as follow. We present the low-dimensional dynamical system in Sec. 2. We classify and characterize the first and second transitions in Sec. 3. Numerical results corroborating the analysis are given in Sec. 4. We conclude the article with some physical implications in Sec. 5.

2. The mathematical formulation

In this section, we give a quick derivation of the low-dimensional dynamical system from the Boussinesq system governing the RB convection in an incompressible conducting fluid subject to a vertical magnetic field in a 2D channel. The derivation follows closely that of the Lorentz system [25], see also [26]. The 2D Boussinesq system is as follows

$$\frac{\partial \mathbf{u}}{\partial t} + (\mathbf{u}\cdot\nabla)\mathbf{u} = \nu\Delta\mathbf{u} - \frac{1}{\rho_0}\nabla p^* + \frac{\mu_0}{\rho_0}(\mathbf{H}\cdot\nabla)\mathbf{H} - g\mathbf{k}(1-\alpha(T-T_0)), \tag{1}$$

$$\frac{\partial T}{\partial t} + (\mathbf{u}\cdot\nabla)T = \kappa\Delta T, \tag{2}$$

$$\frac{\partial \mathbf{H}}{\partial t} + (\mathbf{u}\cdot\nabla)\mathbf{H} = \eta\Delta\mathbf{H} + (\mathbf{H}\cdot\nabla)\mathbf{u}, \tag{3}$$

$$\nabla\cdot\mathbf{u} = 0, \tag{4}$$

$$\nabla\cdot\mathbf{H} = 0, \tag{5}$$

where $\Delta = \frac{\partial^2}{\partial x^2} + \frac{\partial^2}{\partial z^2}$ is the 2D Laplacian; $\mathbf{u}, T, \mathbf{H}$ are the velocity field, temperature field, and magnetic field respectively; and p^* is the modified pressure $p^* = p + \frac{\mu_0}{2}\mathbf{H}^2$. In the system, ν is the kinematic viscosity, μ_0 is the magnetic permeability, g is the gravitational constant, α is the coefficient of volume expansion, κ is the thermal diffusivity, and η is the magnetic diffusivity.

The system (1) can be reformulated in terms of stream functions. Upon making the transformation

$$\mathbf{u} = \left(-\frac{\partial\psi}{\partial z}, \frac{\partial\psi}{\partial x}\right), \tag{6}$$

$$\mathbf{H} = H_0\mathbf{k} + \left(-\frac{\partial\phi}{\partial z}, \frac{\partial\phi}{\partial x}\right), \tag{7}$$

$$T = T_0 + (T_1 - T_0)\frac{z}{h} + \Theta, \tag{8}$$

the system (1) becomes

$$\frac{\partial\Delta\psi}{\partial t}+\frac{\partial(\psi,\Delta\psi)}{\partial(x,z)}=\nu\Delta^2\psi+\frac{\mu_0}{\rho_0}\frac{\partial(\phi,\Delta\phi)}{\partial(x,z)}+\frac{\mu_0}{\rho_0}H_0\frac{\partial\Delta\phi}{\partial z}+g\alpha\frac{\partial\Theta}{\partial x}, \tag{9}$$

$$\frac{\partial\Theta}{\partial t}+\frac{\partial(\psi,\Theta)}{\partial(x,z)}=\kappa\Delta\Theta+\frac{T_0-T_1}{h}\frac{\partial\psi}{\partial x}, \tag{10}$$

$$\frac{\partial\Delta\phi}{\partial t}+\frac{\partial(\psi,\Delta\phi)}{\partial(x,z)}-\frac{\partial(\phi,\Delta\psi)}{\partial(x,z)}=\eta\Delta^2\phi+H_0\frac{\partial\Delta\psi}{\partial z} \tag{11}$$

$$-2\left(\frac{\partial\left(\frac{\partial\psi}{\partial x},\frac{\partial\phi}{\partial x}\right)}{\partial\left(x,z\right)}+\frac{\partial\left(\frac{\partial\psi}{\partial z},\frac{\partial\phi}{\partial z}\right)}{\partial\left(x,z\right)}\right), \tag{12}$$

where $\frac{\partial(f,g)}{\partial(x,z)}=\frac{\partial f}{\partial x}\frac{\partial g}{\partial z}-\frac{\partial f}{\partial z}\frac{\partial g}{\partial x}$.

Introducing the dimensionless variables with h the height of the channel

$$(x,z)=h(x',z'),t=\frac{h^2}{\kappa}t',\psi=\kappa\psi',\phi=hH_0\phi', \tag{13}$$

and defining the dimensionless constants

$$P_r=\frac{\nu}{\kappa},\qquad \text{the Prandtl number}, \tag{14}$$

$$P_m=\frac{\eta}{\kappa},\qquad \text{the magnetic Prandtl number}, \tag{15}$$

$$Q=\frac{\mu_0H_0^2h^2}{\rho_0\kappa\nu},\qquad \text{the Chandrasekhar number}, \tag{16}$$

$$R_e=\frac{g\alpha(T_0-T_1)h^2}{\kappa\nu},\qquad \text{the Rayleigh number}, \tag{17}$$

we obtain the following nondimensionalized system, omitting the primes,

$$\frac{1}{P_r}\frac{\partial\Delta\psi}{\partial t}+\frac{1}{P_r}\frac{\partial(\psi,\Delta\psi)}{\partial(x,z)}=\Delta^2\psi+Q\frac{\partial(\phi,\Delta\phi)}{\partial(x,z)}+Q\frac{\partial\Delta\phi}{\partial z}+R_e\frac{\partial\Theta}{\partial x}, \tag{18}$$

$$\frac{\partial\Theta}{\partial t}+\frac{\partial(\psi,\Theta)}{\partial(x,z)}=\Delta\Theta+\frac{\partial\psi}{\partial x}, \tag{19}$$

$$\frac{\partial\Delta\phi}{\partial t}+\frac{\partial(\psi,\Delta\phi)}{\partial(x,z)}-\frac{\partial(\phi,\Delta\psi)}{\partial(x,z)}=P_m\Delta^2\phi+\frac{\partial\Delta\psi}{\partial z} \tag{20}$$

$$-2\left(\frac{\partial\left(\frac{\partial\psi}{\partial x},\frac{\partial\phi}{\partial x}\right)}{\partial\left(x,z\right)}+\frac{\partial\left(\frac{\partial\psi}{\partial z},\frac{\partial\phi}{\partial z}\right)}{\partial\left(x,z\right)}\right). \tag{21}$$

In order to study the transition of system (18), we use the following mode truncation

$$\psi=X(t)\sin a\pi x\sin\pi z, \tag{22}$$

$$\phi=W(t)\sin a\pi x\cos\pi z, \tag{23}$$

$$\Theta=Y(t)\cos a\pi x\sin\pi z-Z(t)\sin 2\pi z. \tag{24}$$

with $a = \frac{h}{l}$ the aspect ratio of the channel. Plugging (22)-(24) into system (18) and comparing coefficients, an ODE system resembling a Lorentz type equation with a magnetic field can be obtained, see [26] :

$$\frac{dX}{dt} = -P_r X + P_r Y - P_r Q W, \tag{25}$$

$$\frac{dY}{dt} = RX - Y - XZ, \tag{26}$$

$$\frac{dZ}{dt} = -BZ + XY, \tag{27}$$

$$\frac{dW}{dt} = cP_r P_m^{-1} X - P_r P_m^{-1} W, \tag{28}$$

where we have introduced the geometric constants

$$B = \frac{4}{1+a^2}, c = \frac{1}{\pi^2}\frac{1}{(1+a^2)^2}, \tag{29}$$

and a normalized Rayleigh number $R = \frac{R_e}{R_c}$ relative to the critical Rayleigh number R_c. Hereafter we focus on the study of dynamic transitions of (25) as the Rayleigh number R and the Chandrasekhar number Q vary. Furthermore, we take

$$P_r = P_m = 10, \tag{30}$$

in order to be consistent with Lorenz's original result without magnetic field. Throughout, we study the system

$$\frac{dX}{dt} = -10X + 10Y - 10QW, \tag{31}$$

$$\frac{dY}{dt} = RX - Y - XZ, \tag{32}$$

$$\frac{dZ}{dt} = -BZ + XY, \tag{33}$$

$$\frac{dW}{dt} = \frac{B^2}{16\pi^2} X - W. \tag{34}$$

3. Classification of the dynamical transitions

3.1. First transition

It is easy to see that (31)–(34) has a global attractor. In fact, a Lyapunov function for this system is given by

$$V = \frac{1}{2}\left(x^2 + y^2 + (z - 10 - R)^2 + \frac{160\pi^2 Q}{B^2} w^2\right). \tag{35}$$

Indeed, we have

$$\begin{aligned}\tfrac{dV}{dt} &= \tfrac{\partial V}{\partial x}\tfrac{dx}{dt} + \tfrac{\partial V}{\partial y}\tfrac{dy}{dt} + \tfrac{\partial V}{\partial z}\tfrac{dz}{dt} + \tfrac{\partial V}{\partial w}\tfrac{dw}{dt} \\ &= -10x^2 - y^2 - B\left(z - 5 - \tfrac{R}{2}\right)^2 - \tfrac{160\pi^2 Q}{B^2}w^2 + \tfrac{B}{4}(10+R)^2,\end{aligned}$$

from which it follows that

$$\left\{(x,y,z,w)\,\middle|\,10x^2 + y^2 + B\left(z - 5 - \frac{R}{2}\right)^2 + \frac{160\pi^2 Q}{B^2}w^2 \le \frac{B}{4}(10+R)^2\right\}$$

is a absorbing set for (31)–(34) , and so the existence of a global attractor is established.

Regarding the transition of the system at the equilibrium point $P_0 = (0,0,0,0)$, we begin by noting that the corresponding linearization is governed by the matrix

$$L_R = \begin{pmatrix} -10 & 10 & 0 & -10Q \\ R & -1 & 0 & 0 \\ 0 & 0 & -B & 0 \\ \frac{B^2}{16\pi^2} & 0 & 0 & -1 \end{pmatrix}. \tag{36}$$

The corresponding eigenvalues are found to be

$$\lambda_2 = -1, \lambda_3 = -B, \tag{37}$$

$$\lambda_4 = \tfrac{-\sqrt{2}\sqrt{-5B^2Q + 80\pi^2 R + 162\pi^2} - 22\pi}{4\pi}, \tag{38}$$

$$\lambda_1 = \tfrac{\sqrt{2}\sqrt{-5B^2Q + 80\pi^2 R + 162\pi^2} - 22\pi}{4\pi}. \tag{39}$$

In virtue of (37) we see that the following holds:

$$\lambda_1(R,Q)\begin{cases} < 0, R < R_1, \\ = 0, R = R_1, \\ > 0, R > R_1, \end{cases} \tag{40}$$

$$\lambda_i(R_1,Q) < 0, i = 2,3,4, R_1 = 1 + \tfrac{B^2 Q}{16\pi^2} \tag{41}$$

These conditions are referred to as the principle exchange of stability in the dynamic phase transition theory, cf. [27]. We are thus led to the following result.

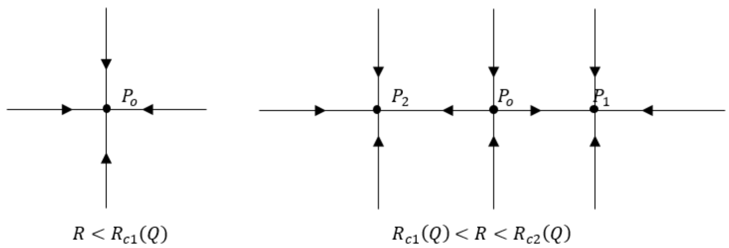

Figure 1: Topological structure of the first transition. P_0 is the origin; P_1 and P_2 are the bifurcated solutions defined in Eqs. (42)-(43); R is the Rayleigh number; R_1 and R_2 are the first and second critical Rayleigh number, respectively; arrow lines indicated stability.

Theorem 3.1. *The system* (31)–(34) *undergoes a continuous transition around the origin at $R = R_1$. More precisely, for $R \leq R_1$ and $Q < \frac{48\pi^2}{B^2}$, There exists R_0 dependent on B and Q such that if $R \leq R_0 \leq R_1$, the origin $P_0 = (0, 0, 0, 0)$ is the only fixed point of the system and it attracts any bounded set in R^4, whereas for $R > R_1$, P_0 bifurcates to two non-trivial solutions given by*

$$P_1 = \left(\sqrt{\frac{B(R-C)}{C}}, \sqrt{B(R-C)C}, R-C, \frac{B^2}{16\pi^2}\sqrt{\frac{B(R-C)}{C}}\right), \tag{42}$$

$$P_2 = \left(-\sqrt{\frac{B(R-C)}{C}}, -\sqrt{BC(R-C)}, R-C, -\frac{B^2}{16\pi^2}\sqrt{\frac{B(R-C)}{C}}\right), \tag{43}$$

where $C = 1 + \frac{B^2 Q}{16\pi^2}$. Furthermore, the critical points P_1 and P_2 are stable, and there exists two disjoint open sets U_1, U_2, with $R^4 = \bar{U_1} \cup \bar{U_2}, \partial U_1 \cap \partial U_2 = \Gamma$, where U_i is the basin of attraction of P_i for $i = 1, 2$, and Γ is the stable manifold of P_0.

The topological structure of the first transition around P_0 is shown in Fig. (1).

Proof. At the critical value $R = R_1$, the eigenvectors of (36) corresponding to the eigenvalues given in (37) are given (in row form for conciseness of notation) by

$$
\begin{aligned}
e_1 &= \left(-\frac{10}{M}, Q+\frac{1}{M}, 0, 1\right), e_2 = (0, Q, 0, 1), \\
e_3 &= (0,0,1,0), e_4 = \left(\frac{1}{M}, Q+\frac{1}{M}, 0, 1\right), M = \frac{B^2}{16\pi^2}.
\end{aligned}
$$

Similarly, the dual eigenvectors (i.e. left eigenvectors of L_R) are given by

$$
\begin{aligned}
e_1^* &= \left(\frac{1}{Q}, -\frac{1}{Q}, 0, 1\right), e_{2^*} = \left(\frac{-M}{1+MQ}, Q, 0, 1\right), \\
e_3^* &= (0,0,1,0), e_4^* = \left(\frac{-1}{10Q}, \frac{-1}{Q}, 0, 1\right).
\end{aligned}
$$

Now, let $E_1 = \text{span}\ \{e_1\}$, $E_2 = \text{span}\ \{e_2, e_3, e_4\}$, and $\mathcal{P}_2$ be the projection onto E_2. Based on the approximate formula for the center manifold in [27] (Appendix A, equation (A.2.19)), the linearization around P_0 behaves like $u = xe_1 + \Phi + o(x^2)$, where Φ is determined by the equation

$$
-L_R\Phi = \mathcal{P}_2 G(e_1, e_1)x^2. \tag{44}
$$

Here L_R is the matrix defined in (36).

More precisely, writing $\Phi = (a_2e_2 + a_3e_3 + a_4e_4)x^2 + o(x^2)$, (44) takes the form

$$
(-L_R(a_2e_2 + a_3e_3 + a_4e_4), e_i^*) = (G(e_1, e_1), e_i^*), i = 2, 3, 4. \tag{45}
$$

It is easy to see that the unique solution of (45) is given by

$$
a_2 = a_4 = 0, a_3 = -\frac{1}{B}\left(\frac{10}{M^2} + \frac{10Q}{M}\right). \tag{46}
$$

The invariant manifold function is thus approximately given by

$$
\Phi = -\frac{1}{B}\left(\frac{10}{M^2} + \frac{10Q}{M}\right) x^2 e_3 + o(x^2).
$$

Next, in order to obtain the corresponding reduced equations, we compute

$$
(G(xe_1 + \Phi, xe_1 + \Phi), e_1^*) = -\frac{1}{BQ}\left(\frac{100}{M^3} + \frac{100Q}{M^2}\right) x^3 + o(x^3).
$$

Based on Theorem 2.3.1 in [27], since the coefficient of x^3 above is always negative, it follows that (31)–(34) has a continuous transition at $(0, R_c)$. In other words, the equilibrium P_0 undergoes a pitchfork bifurcation at $R = R_1$.

Now, let's prove the global stability of $\mathbf{0}$. Construct a energy function V as follows

$$V = \left(\frac{1}{10} + \frac{B^2Q}{160\pi^2}\right) X^2 + Y^2 + Z^2 + \left(Q + \frac{16\pi^2}{B^2}\right) QW^2. \tag{47}$$

Then, we have

$$\begin{aligned}
\frac{dV}{dt} &= 2\left(\frac{1}{10} + \frac{B^2Q}{160\pi^2}\right) X\dot{X} + 2Y\dot{Y} + 2Z\dot{Z} + 2\left(Q + \frac{16\pi^2}{B^2}\right) QW\dot{W} \\
&= -2\left(1 + \frac{B^2Q}{16\pi^2}\right) X^2 + 2\left(R + 1 + \frac{B^2Q}{16\pi^2}\right) XY - 2Y^2 \\
&- 2BZ^2 - 2\left(Q + \frac{16\pi^2}{B^2}\right) QW^2 \\
&= -2\left(1 + \frac{B^2Q}{16\pi^2}\right)\left(X^2 - \left(1 + \frac{R}{1 + \frac{B^2Q}{16\pi^2}}\right) XY\right) \\
&- 2Y^2 - 2BZ^2 - 2\left(Q + \frac{16\pi^2}{B^2}\right) QW^2 \\
&= -2\left(1 + \frac{B^2Q}{16\pi^2}\right)\left(X - \frac{1}{2}\left(1 + \frac{R}{1 + \frac{B^2Q}{16\pi^2}}\right) Y\right)^2 \\
&+ \left(\frac{\left(R + 1 + \frac{B^2Q}{16\pi^2}\right)^2}{2 + \frac{B^2Q}{8\pi^2}} - 2\right) Y^2 - 2\left(Q + \frac{16\pi^2}{B^2}\right) QW^2.
\end{aligned} \tag{48}$$

(48) means that

$$\frac{\left(R + 1 + \frac{B^2Q}{16\pi^2}\right)^2}{2 + \frac{B^2Q}{8\pi^2}} - 2 \leq 0 \tag{49}$$

is the sufficient condition of the global stability of $\mathbf{0}$, and $Q < \frac{48\pi^2}{B^2}$, means that

$$R_1 \geq R_0 = -1 - \frac{B^2Q}{16\pi^2} + 2\sqrt{1 + \frac{B^2Q}{16\pi^2}} > 0. \tag{50}$$

$\square$

3.2. Second transition

In this section we study the transition from the bifurcated equilibria P_i, $i = 1, 2$, occurring when $R > R_1$ is sufficiently large. Hereafter we consider the transformation

$$(X, Y, Z, W) = P_1 + (X', Y', Z', W'),$$

so that, upon substitution in (31)–(34) and dropping the primes, we obtain the system

$$\frac{dX}{dt} = -10X + 10Y - 10QW, \tag{51}$$

$$\frac{dY}{dt} = CX - Y - \sqrt{\frac{B(R-C)}{C}}Z - XZ, \tag{52}$$

$$\frac{dZ}{dt} = \sqrt{B(R-C)C}X + \sqrt{\frac{B(R-C)}{C}}Y - BZ + XY, \tag{53}$$

$$\frac{dW}{dt} = \frac{B^2}{16\pi^2}X - W. \tag{54}$$

Note that there is no loss of generality in considering only P_1, since by performing the analogous transformation

$$(X, Y, Z, W) = P_2 + (X', Y', Z', W'),$$

one arrives again at (51)–(54).

By linearizing (51)–(54) around the origin one obtains the matrix

$$\mathbb{M} = \begin{pmatrix} -10 & 10 & 0 & -10Q \\ D & -1 & -\sqrt{\frac{B(R-C)}{C}} & 0 \\ \sqrt{B(R-C)C} & \sqrt{\frac{B(R-C)}{C}} & -B & 0 \\ \frac{B^2}{16\pi^2} & 0 & 0 & -1 \end{pmatrix}. \tag{55}$$

The eigenvalues of $\mathbb{M}$ are determined by the equation

$$\lambda^4 + a_3\lambda^3 + a_2\lambda^2 + a_1\lambda + a_0 = 0$$

where, after some straightforward computations, we obtain the formulae

$$\begin{aligned} a_3 &= B + 12, \\ a_2 &= 11(B+1) + \frac{BR}{\frac{B^2}{16\pi^2}Q + 1}, \\ a_1 &= \frac{11}{\frac{B^2}{16\pi^2}Q + 1}BR + 10B\left(R - \frac{B^2}{16\pi^2}Q - 1\right), \\ a_0 &= 20B\left(R - \frac{B^2}{16\pi^2}Q - 1\right). \end{aligned}$$

The above quartic equation has a purely imaginary solution if and only if

$$a_1^2 + a_0 a_3^2 = a_1 a_2 a_3$$

which in turns becomes a quadratic equation for R whose unique solution greater than R_1 is of the form

$$R_2 = \frac{25(B^2Q + 16\pi^2)}{D}\left[\frac{4\pi^2}{25}(B+12)\sqrt{Y_1} + Y_2\right]$$

where

$$\begin{aligned}
Y_1 &= \left(2500\,B^6 - 4300\,B^5 + 4225\,B^4\right)Q^2\\
&+ \left(173280\,B^4\pi^2 - 170160\,B^3\pi^2 + 9360\,\pi^2 B^2\right)Q\\
&+ 3069504\,B^2\pi^4 + 252288\,B\pi^4 + 5184\,\pi^4,\\
Y_2 &= \frac{1}{25}\left(6432\,B^2 + 90336\,B - 3456\right)\pi^4\\
&+ \frac{32\,B^2\pi^2 Q}{5}\left(B^2 + \frac{145\,B}{8} - \frac{39}{2}\right) + B^5Q^2,\\
D &= 400B^5Q^2\pi^2 - 640B^3Q(B-30)\pi^4 - 21504(B-9)B\pi^6.
\end{aligned}$$

It is easy to see from the above formulae that for any fixed pair (Q, B) there exists a unique R_2 such that

$$\text{Re } x_i \begin{cases} < 0, & R < R_2, \\ = 0, & R = R_2, \quad i = 1, 2, \\ > 0, & R > R_2, \end{cases} \tag{56}$$

$$\text{Re } x_i < 0, i = 3, 4, \tag{57}$$

$$\text{Im } x_i \neq 0, i = 1, 2. \tag{58}$$

The values of R and Q that give raise to the first and second transitions as discussed above are shown in Fig. 2, where the value of B is fixed at $8/3$, which corresponds to the spatial scale $L = \sqrt{2}$.

3.2.1. The type of second transition

We use the transition theorem established by Ma and Wang [27] to study type of transition for problem (31)–(34). Before doing so, we focus on some analysis.

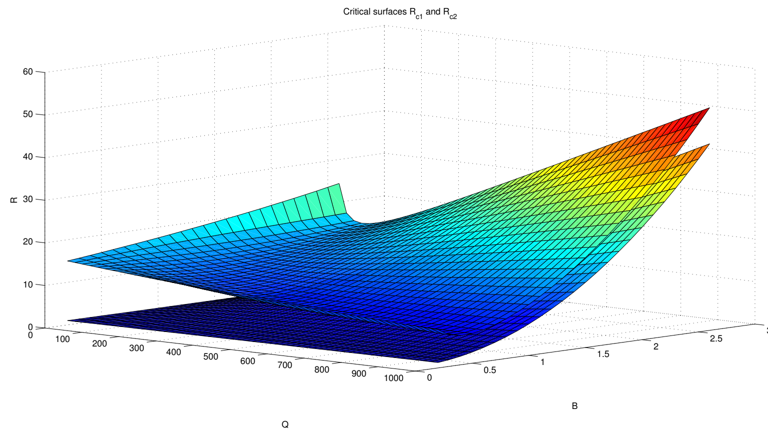

Figure 2: Neutral surfaces R_1 (lower surface) and R_2 (upper surface) as functions of Q (x-axis) and B(y-axis).

Denote

$$G(X,Y,Z,W) \quad = \quad \begin{pmatrix} 0 \\ -XZ \\ XY \\ 0 \end{pmatrix}. \tag{59}$$

Let $\{\beta_k(R)\}_{k=1}^4$ be the eigenvalues of the matrix $\mathbb{M}$ given in (55), and assume $\beta_1 = \alpha - i\sigma = \overline{\beta_2}$, and $\beta_3, \beta_4 \in \mathbb{R}$. Let e_1 and e_2 be the real part and imaginary part of the eigenvector corresponding to β_1, respectively. For $\xi = xe_1 + ye_2$ we have

$$\mathbb{M}\xi = (\alpha x - \sigma y)e_1 + (\alpha y + \sigma x)e_2.$$

We introduce the linear spaces $H_c = \text{span}\,\{e_1, e_2\}$ and $H_s = \{e_3, e_4\}$, with corresponding orthogonal projections P_c and P_s. Letting $u = xe_1 + ye_2 + ze_3 + we_4$, $u_c = P_c u$ and $u_s = P_s u$, one can rewrite (51)–(54) as

$$\begin{aligned}
\frac{dx}{dt} &= \alpha x - \sigma y + (G(u_c + u_s, u_c + u_s), e_1^*)\,, \\
\frac{dy}{dt} &= (\alpha y + \sigma x) + (G(u_c + u_s, u_c + u_s), e_2^*)\,, \\
\frac{du_s}{dt} &= \mathbb{M}_s u_s + P_s G(u_c + u_s, u_c + u_s).
\end{aligned}$$

In order to approximate the center manifold function we use the ansatz

$$u_s = h(u_c) = h_2(u_c) + h_3(u_c) + h_4(u_c) + O(|u_c|^5),$$

where h_k is k-linear. Note that

$$\frac{du_s}{dt} = \frac{dh}{dt} = \partial_x h \frac{dx}{dt} + \partial_y h \frac{dy}{dt}$$

which means that

$$\begin{aligned}
&\mathbb{M}_s h + G_s(u_c, u_c) + \tilde{G}_s(u_c, h) + G_s(h, h) \\
&= \partial_x h \left[\alpha x - \sigma y + (G(u_c + u_s, u_c + u_s), e_1^*)\right] \\
&\quad + \partial_y h \left[\alpha y + \sigma x + (G(u_c + u_s, u_c + u_s), e_2^*)\right]
\end{aligned}$$

Now, for $h = f_3(x, y)e_3 + f_4(\bar{x}, \bar{y})e_4$, let's define

$$\nabla h(u_c) \equiv \begin{pmatrix}
e_{3,1}\left(\frac{\partial f_3}{\partial x} e_1^{*T} + \frac{\partial f_3}{\partial y} e_2^{*T}\right) + e_{4,1}\left(\frac{\partial f_4}{\partial x} e_1^{*T} + \frac{\partial f_4}{\partial y} e_2^{*T}\right) \\
e_{3,2}\left(\frac{\partial f_3}{\partial x} e_1^{*T} + \frac{\partial f_3}{\partial y} e_2^{*T}\right) + e_{4,2}\left(\frac{\partial f_4}{\partial x} e_1^{*T} + \frac{\partial f_4}{\partial y} e_2^{*T}\right) \\
e_{3,3}\left(\frac{\partial f_3}{\partial x} e_1^{*T} + \frac{\partial f_3}{\partial y} e_2^{*T}\right) + e_{4,3}\left(\frac{\partial f_4}{\partial x} e_1^{*T} + \frac{\partial f_4}{\partial y} e_2^{*T}\right) \\
e_{3,4}\left(\frac{\partial f_3}{\partial x} e_1^{*T} + \frac{\partial f_3}{\partial y} e_2^{*T}\right) + e_{4,4}\left(\frac{\partial f_4}{\partial x} e_1^{*T} + \frac{\partial f_4}{\partial y} e_2^{*T}\right)
\end{pmatrix}.$$

Let $u_c = xe_1 + ye_2$, above equations can be rewritten as the following normal form

$$\begin{aligned}
&\nabla h_2 \mathbb{M}_c \xi + \nabla h_3 \mathbb{M}_c \xi + \nabla h_2 G_c(\xi, \xi) \\
&+ \nabla h_4 \mathbb{M}_c \xi + \nabla h_2 \tilde{G}_c(\xi, h_2) + \nabla h_3 G_c(\xi, \xi) \\
&= \mathbb{M}_s h_2 + G_s(\xi, \xi) + \mathbb{M}_s h_3 + \tilde{G}_s(\xi, h_2) \\
&+ \mathbb{M}_s h_4 + \tilde{G}_s(\xi, h_3) + G_s(h_2, h_2) + O(|\xi|^5).
\end{aligned}$$

The quadratic part of the above identity gives

$$\nabla h_2 \mathbb{M}_c \xi - \mathbb{M}_s h_2 = G_s(\xi, \xi).$$

The formula for h_2 is then found by simply solving a linear system. More precisely, letting $h_2(\xi) = \sum_{i=3}^4 (x^2 \phi^i_{2,0} + xy\phi^i_{1,1} + y^2 \phi^i_{0,2})e_i$ and $\phi^i = (\phi^i_{2,0}, \phi^i_{1,1}, \phi^i_{0,2})^T$, one needs to solve

$$(N_2 - \beta_i)\phi^i = \begin{pmatrix} \langle G(e_1, e_1), e_i^* \rangle \\ \left\langle \tilde{G}(e_1, e_2), e_i^* \right\rangle \\ \langle G(e_2, e_2), e_i^* \rangle \end{pmatrix},$$

where

$$N_2 = \begin{pmatrix} 2\alpha & \sigma & 0 \\ -2\sigma & 2\alpha & 2\sigma \\ 0 & -\sigma & 2\alpha \end{pmatrix}.$$

Similar but more complicated formulas can also be obtained for h_3 and h_4 without much work. Thus, besides inverting the above linear system, finding the explicit form of the eigendecomposition constitutes the core of the computational work needed to reduce the system.

After having performed all these calculations we arrive at a set of reduced equations of the form

$$\frac{dx}{dt} = \alpha x - \sigma y + \sum_{2 \le p+q \le 5} a^1_{pq} x^p y^q + O(|(x, y)|^6), \tag{60}$$

$$\frac{dy}{dt} = \alpha y + \sigma x + \sum_{2 \le p+q \le 5} a^2_{pq} x^p y^q + O(|(x, y)|^6), \tag{61}$$

where the coefficients a^i_{pq}, $i = 1, 2$, $2 \le p+q \le 5$, can be determined numerically by using the procedure outlined above.

In the polar coordinate $x = r\cos\theta, y = r\sin\theta$, we derive from the system (60) –(61) that

$$\frac{dr}{d\theta} = \frac{\alpha r + \sum_{k=2}^{5} r^k u_k(\sin\theta, \cos\theta) + o(r^5)}{\sigma - \sum_{k=2}^{5} r^{k-1} v_k(\sin\theta, \cos\theta) + o(r^4)}, \tag{62}$$

where

$$u_k(\sin\theta, \cos\theta) = \sum_{p+q=k} a^1_{pq} \cos^{p+1}\theta \sin^q\theta + a^2_{pq} \cos^p\theta \sin^{q+1}\theta,$$

$$v_k(\sin\theta, \cos\theta) = \sum_{p+q=k} a^1_{pq} \cos^p\theta \sin^{q+1}\theta - a^2_{pq} \cos^{p+1}\theta \sin^q\theta.$$

Near $r = 0$, (62) can be expressed as

$$\frac{1}{r^2}\frac{dr}{d\theta} = \frac{1}{\sigma}\left(\frac{\alpha}{r} + \sum_{k=2}^{5} r^{k-2} f_k(\sin\theta, \cos\theta) + o(r^3),\right) \tag{63}$$

where

$$\begin{aligned}
f_2 &= u_2 + \sigma^{-1}\alpha v_2,\\
f_3 &= u_3 + \sigma^{-1}\alpha v_3 + \sigma^{-1}u_2 v_2 + \sigma^{-2}\alpha v_2^2,\\
f_4 &= u_4 + \sigma^{-1}\alpha v_4 + \sigma^{-1}u_2 v_3 + \sigma^{-1}u_3 v_2\\
&\quad + 2\sigma^{-2}\alpha v_2 v_3 + \sigma^{-2}u_2 v_2^2 + \sigma^{-3}\alpha v_2^3,\\
f_5 &= u_5 + \sigma^{-1}\alpha v_5 + \sigma^{-1}u_2 v_4 + \sigma^{-1}u_3 v_3 + \sigma^{-1}u_4 v_2\\
&\quad + \alpha\sigma^{-2}v_3^2 + 2\sigma^{-2}\alpha v_2 v_4 + 2\sigma^{-2}u_2 v_2 v_3 + \sigma^{-1}u_3 v_2^2\\
&\quad + 3\sigma^{-3}\alpha v_2^2 v_3 + \sigma^{-3}u_2 v_3^3 + \sigma^{-4}\alpha v_3^4,
\end{aligned}$$

with the initial value

$$r(0, R, Q, B) = a.$$

Let $r(\theta, R, Q, B, a)$ have the following Taylor expansion with respect to a at 0

$$r(\theta, R, Q, B, a) = a + d_2(\theta, R, Q, B)a^2 + d_3(\theta, R, Q, B)a^3 + o(a^3). \tag{64}$$

Putting (64) into (63) gives

$$\frac{dr}{d\theta} = \frac{\alpha}{\sigma}a + \left(\frac{\alpha}{\sigma}d_2 + f_2/\sigma\right)a^2 + \left(\frac{\alpha}{\sigma}d_3 + 2d_2 f_2/\sigma + f_3/\sigma\right)a^3 + o(a^3). \tag{65}$$

Integrating respect to θ gives

$$\begin{aligned}
r(\theta, R, Q, B) =& a + \frac{a^2}{\sigma}\int_0^\theta f_2 ds + \frac{a^3}{\sigma}\int_0^\theta (2d_2 f_2 + f_3) ds\\
&+ a^2\int_0^\theta \frac{\alpha}{\sigma}d_2 ds + a^3\int_0^\theta \frac{\alpha}{\sigma}d_3 ds + \frac{\alpha}{\sigma}\theta a.
\end{aligned} \tag{66}$$

Comparing with (64), we see that

$$\begin{aligned}
d_2 &= \frac{1}{\sigma}\int_0^\theta f_2 ds,\\
d_3 &= \frac{1}{\sigma}\int_0^\theta (2d_2 f_2 + f_3) ds.
\end{aligned} \tag{67}$$

Using (67), and integrating (63) from 0 to 2π, we obtain

$$\begin{aligned}
&\frac{r(2\pi,a)-r(0,a)}{r(2\pi,a)} \\
&= \frac{\alpha\rho}{\sigma} + \frac{a}{\sigma}\int_0^{2\pi} f_2 d\theta + \frac{a^2}{\sigma}\int_0^{2\pi} f_3 d\theta \\
&\quad + \frac{a^3}{\sigma}\int_0^{2\pi}\left(f_4 + f_3\left(\int_0^{\theta} f_2 ds\right)\right) d\theta \\
&\quad + \frac{a^4}{\sigma}\int_0^{2\pi}\left(f_5 + 2f_4\left(\int_0^{\theta} f_2 ds\right) + f_3\left(\int_0^{\theta} f_3 ds\right)\right) d\theta \\
&\quad + \frac{2a^4}{\sigma}\int_0^{2\pi} f_3\left(\int_0^{\theta} f_2\left(\int_0^{\theta} f_2 ds\right) ds\right) d\theta,
\end{aligned} \tag{68}$$

where $\rho = 2\pi + o(a)$. Direct computation gives that

$$\begin{aligned}
&\int_0^{2\pi} f_2 d\theta = 0, \\
&\int_0^{2\pi} f_4 d\theta = 0, \\
&\int_0^{2\pi} f_3\left(\int_0^{\theta} f_2 ds\right) d\theta = \frac{2}{3}a_{02}^2\int_0^{2\pi} f_3 d\theta + o(a), \\
&\int_0^{2\pi} f_3\left(\int_0^{\theta} f_3 ds\right) d\theta = 0.
\end{aligned} \tag{69}$$

Thus, (68) can be rewritten as

$$\frac{r(2\pi,a)-r(0,a)}{r(2\pi,a)} = \frac{\rho\alpha}{\sigma} + \delta_2 a^2 + \delta_3 a^3 + \delta_4 a^4 + o(a^4), \tag{70}$$

where

$$\begin{aligned}
\delta_2 &= \int_0^{2\pi} f_3 d\theta, \\
\delta_3 &= \frac{2}{3}a_{02}^2\delta_2, \\
\delta_4 &= \int_0^{2\pi}\left(f_5 + 2f_4\left(\int_0^{\theta} f_2 ds\right)\right) d\theta \\
&\quad + \int_0^{2\pi} f_3\left(\int_0^{\theta} f_2\left(\int_0^{\theta} f_2 ds\right) ds\right) d\theta.
\end{aligned} \tag{71}$$

It is known that each real positive zero a_0 of Eq. (70) corresponds to a periodic solution of (60)–(61). Given a periodic orbit with the fixed a_0, for all a close to

a_0, if

$$r(2\pi, a) - r(0, a) \begin{cases} < 0, & a > a_0, \\ > 0, & a < a_0, \end{cases} \tag{72}$$

then the periodic orbit associated with a_0 is stable; otherwise, if

$$r(2\pi, a) - r(0, a) \begin{cases} > 0, & a > a_0, \\ < 0, & a < a_0, \end{cases} \tag{73}$$

then the periodic orbit is unstable.

Denote

$$N = \frac{\rho\alpha}{\sigma} + \delta_2 a^2 + \delta_3 a^3 + \delta_4 a^4 + o(a^4). \tag{74}$$

For the stability of the critical points P_1 and P_2 at $R = R_2$, we look at the sign of N for small positive a. It is clear that the sign of $\delta_2(R_2)$ determines the stability, as $\alpha = 0$ (the real part of the complex eigenvalue) at $R = R_2$. Hence we define $\delta_2(R_2)$ as the transition number with $\delta_2(R_2) > (<)\ 0$ signifying jump (continuous) transition of the system (31)–(34) at $R = R_2$. If $\delta_2 = 0$ (so is δ_3, cf. Eq. (71)), we can use $\delta_4(R_2)$ as the transition number. See [27] for details. Then we have following results

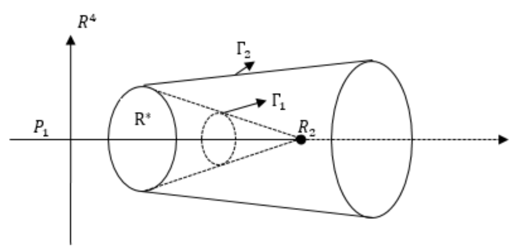

Figure 3: Topological structure of the jump transition $\delta_2(R_2) > 0$. A periodic orbit Γ occurs from P_1 on $R < R_2$. A nonzero attractor appears at R^*.

Theorem 3.2. *If $\delta_2(R_2) > 0$ or $\delta_2(R_2) = 0, \delta_4(R_2) > 0$, the system* (31)–(34) *undergoes a jump transition with an unstable periodic orbit Γ_1 colliding with P_1 and the coexistence of a stable periodic orbit Γ_2 at the second critical number*

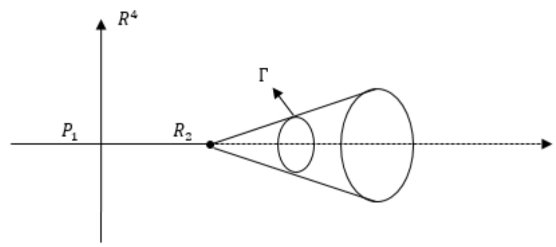

Figure 4: Topological structure of the continuous transition. A Hopf bifurcation occurs at R_2, indicating that a stable limit cycle bifurcates from P_1 at $R = R_2$, and whose size grows continuously with R.

R_2. In addition, there exists a subcritical transition number R^* ($R_0 < R^* \leq R_2$) at which there exists a singular separation of periodic orbits such that nonzero attractor Γ bifurcates from P_1 at $R = R^*$. While there is no periodic solution bifurcating from P_1 when $R > R_2$.

The topological structure of the jump transition in Theorem 3.2 is best described in Fig.3.

Proof. Since the quadratic term in N is the dominant one when $a > 0$ is small, it is clear that P_1 is unstable and the transition is of jump type at $R = R_2$, under the assumption of this theorem. $\delta_2(R_2) > 0$ or $\delta_2(R_2) = 0, \delta_4(R_2) > 0$ implies that N defined in (74) has a real positive root

$$\Gamma = \left(\frac{-\rho\alpha}{\sigma\delta_2} \right)^{\frac{1}{2}} (\delta_2 > 0) \text{ or } \left(\frac{-\rho\alpha}{\sigma\delta_4} \right)^{\frac{1}{4}} (\delta_2 = 0). \tag{75}$$

for $R < R_{2c}$. Using (73) finds that Γ_2 is unstable. At last, Combining the existence of global attractor (see Sec.3.1), results in Theorem 3.1 and the instability of P_1 at $R = R_2$, it means that there exists subcritical number $R = R^*$ such that $R_0 < R^* \leq R_2$, and there is a non-zero attractor occurs at $R = R^*$. The results of separation of periodic orbits can be obtained from the Theorem 2.3.4 and 2.5.1 of Ma and Wang in [27]. □

Theorem 3.3. *If $\delta_2(R_2) \leq 0, \delta_3(R_2) \leq 0$ and $\delta_4(R_2) < 0$, the system (31)–(34) undergoes a continuous transition (a Hopf bifurcation) at $R = R_2$. In particular, the steady-state solution P_1 bifurcates to a stable periodic trajectory Γ on $R > R_2$, i.e.,*

$$\Gamma \to P_1, R \to R_2. \tag{76}$$

Furthermore, the periodic orbit is approximately derived as

$$u(t) = \left(\frac{-\rho\alpha}{\sigma\delta_2}\right)^{\frac{1}{2}} (\cos(\sigma t)e_1 + \sin(\sigma t)e_2) + o(|R - R_c|), \delta_2 > 0, \tag{77}$$

$$u(t) = \left(\frac{-\rho\alpha}{\sigma\delta_4}\right)^{\frac{1}{4}} (\cos(\sigma t)e_1 + \sin(\sigma t)e_2) + o(|R - R_c|), \delta_2 = 0. \tag{78}$$

The topological structure of continuous transition described in Theorem 3.3 is shown in Fig.4.

Proof. Under the assumptions of $\delta_2(R_2) \leq 0, \delta_3(R_2) \leq 0$ and $\delta_4(R_2) < 0$, it is easy to see that N defined in (74) is negative at $R = R_2$ for small a, i.e., any orbit near P_1 converges to P_1. Hence, P_1 is stable at $R = R_2$, and the transition at (P_1, R_2) is of continuous type. In addition, it is clear to see that (74) exactly has only one real positive root

$$\Gamma = \left(\frac{-\rho\alpha}{\sigma\delta_2}\right)^{\frac{1}{2}} (\delta_2 > 0) \text{ or } \left(\frac{-\rho\alpha}{\sigma\delta_4}\right)^{\frac{1}{4}} (\delta_2 = 0). \tag{79}$$

for $R > R_{2c}$. Combining (72) finds that $\Gamma(R)$ is stable. For $R > R_2$, (74) has no root, that is, no periodic solution originates from P_1 on $R > R_2$. $\square$

Remark 3.1. *Above bifurcation and transition are associated with critical P_1, for critical point P_2, the results are same.*

4. Numerical results and discussion

In this section we study numerically the types and structure of the transition that this system exhibits at $R = R_2$ for different values of the geometry parameter B and the Chandrasekhar number Q. According to Eq. (74) the numerical investigation reduces to the computation of the dimensionless numbers

δ_2, δ_3 and δ_4, which can be accomplished by solving a series of linear problems as outlined in Subsection 3.2.1.

Based on Theorems 3.2 and 3.3, a first step in determining the transition type at R_2 is to compute the bifurcation number δ_2. A preliminary exploration of δ_2 in terms of B and Q is shown in Table 1. These results show that the system is

Table 1: The values of the bifurcation number δ_2 with respect to the Chandrasekhar number Q and the geometry parameter B. $\delta_2 > 0$ indicates jump transition; $\delta_2 < 0$ implies continuous transition.

Q$\backslash$ δ_2 $\backslash$ B	0.2	0.4	0.6	0.8	1	1.4
20	0.004	0.0061	0.0070	0.0074	0.0075	0.0073
80	0.0036	0.0052	0.0060	0.0064	0.0068	0.0078
200	0.0026	0.0031	0.0032	0.0036	0.0046	0.0074
600	-0.0014	-0.0058	-0.0067	-0.0041	-0.0005	0.0046
1000	-0.0061	-0.014	-0.0119	-0.0062	-0.0017	0.0031

capable of exhibiting both continuous and jump transitions for different values of Q and B. In view of this fact, a natural subsequent problem is to approximately determine the regions in parameter space that give rise to different types of transition. Since, from a numerical point of view, the evaluation of the map $(Q, B) \mapsto \delta_2$ is relatively straightforward, albeit lengthy, the task just described can be executed without major issues using a bisection method. We thus obtain a curve in parameter space, corresponding approximately to $\delta_2(Q, B) = 0$, that represents an effective boundary between the region where a continuous/jump transition occurs. The results are shown in Figure 5.

From a quantitative point of view, we see that the curve defined by the relation $\delta_2(Q, B) = 0$ can be cast in the form $Q = Q_c(B)$, where Q_c is a convex function defined on the interval (B_0, B_1), with $B_0 = 0$ and $B_1 \approx 1.7795$, and having vertical asymptotes at the endpoints. In particular, for $B_0 < B < B_1$ the type of transition that the system undergoes changes from jump to continuous as Q crosses a threshold given by $Q = Q_c(B)$. Further, when $B \geq B_1$ the transition type at R_2 is always jump, irrespective of the value of Q. We remark

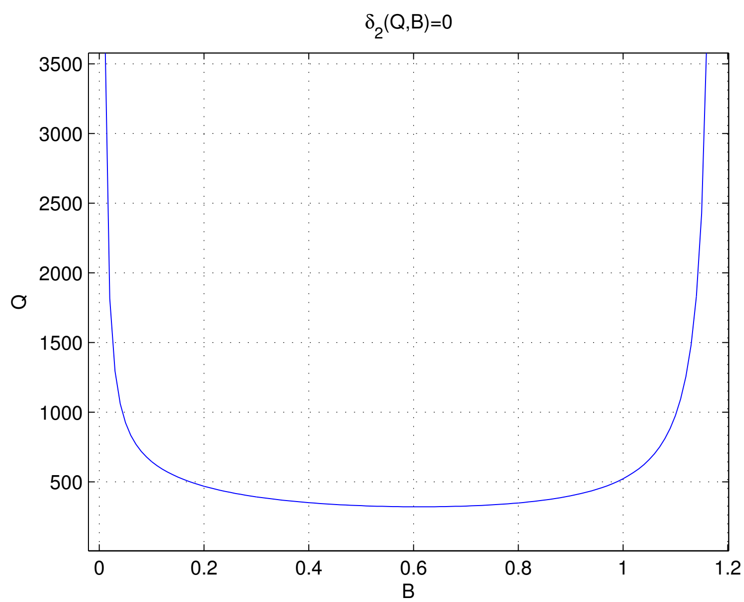

Figure 5: Approximate form of the curve $\delta_2(Q, B) = 0$. Below this curve, the system undergoes a jump transition ($\delta_2 > 0$); above it, the transition is continuous ($\delta_2 < 0$).

that the latter condition is non-trivial, since we have $B = \frac{4}{1+a^2}$, where $a = \frac{h}{l}$ is the height-to-width aspect ratio, so B is allowed to take values up to $B = 4$, and thus the case $B_1 \leq B < 4$ is indeed feasible if a is sufficiently small.

Physically, the above shows that the vertically applied magnetic field plays a stabilizing role in the Rayleigh-Bénard convection. This stabilizing effect is, however, unable to make the transition continuous when the height-to-width ratio is so small that $B > B_1$.

In the case $\delta_2 < 0$ Theorem 3.3 also provides an estimate for the average size of the bifurcated periodic orbit, see (77). On the other hand, one can directly estimate this quantity by solving the main equations (51)–(54) for a sufficiently long time and initial data close to P_1, and a third estimate can also be obtained in the same way by solving instead the reduced equations (60)-(61). Since our analysis predicts that all these quantities are similar to each other, at least for R close to R_2, it is important to corroborate this prediction with numerical simulations. The results are shown in Figure 6. Besides confirming this prediction, the results also show that all three values get closer together as the difference $R - R_2$ decreases, which is in agreement with the analysis.

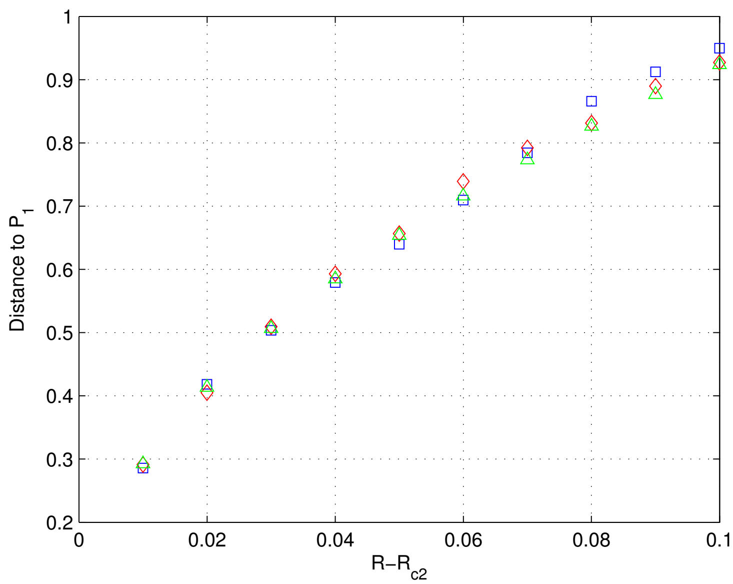

Figure 6: $Q = 1000$, $B = 0.6$. The average distance of the trajectory and the critical point P_1 after long time for full ODE (red), reduced equations (blue), and the predicted theoretical value (green).

Irrespective of the type of transition, the linear analysis predicts that the critical point P_1 is locally asymptotically stable when $R < R_2$. This is corroborated numerically for two sets of parameters producing different types of transitions in Figure 7 (continuous transition) and Figure 8 (jump transition).

In the case $\delta_2 > 0$ the theory predicts the existence of an unstable periodic orbit when $R < R_2$. Since such a solution is unstable, generic numerical simulations are unable to provide insight about its structure. Thus, in order to extract qualitative information regarding this issue, one must turn to the computation of the higher order bifurcation parameters δ_3 and δ_4. In Table 2 we explore some values of the higher order bifurcation numbers for different values of the

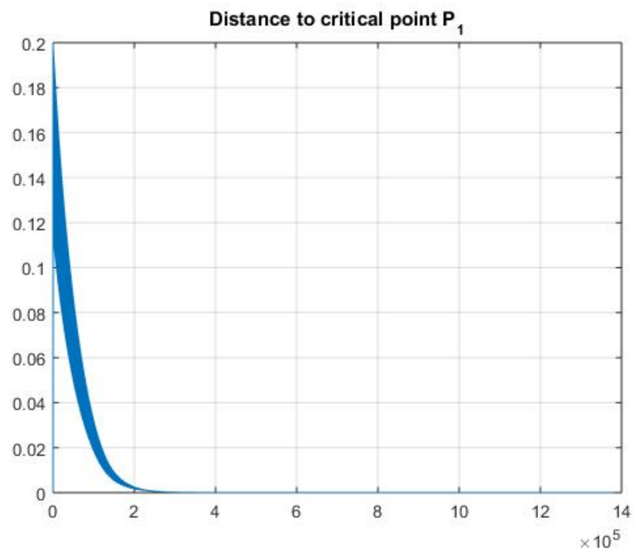

Figure 7: Distance between the trajectory and the critical point P_1 as a function of time before continuous transition, shown for $Q = 1000,\ B = 0.6$.

parameters.

Table 2: $\delta_2 > 0$ and $\delta_4 > 0$ indicate that only one unstable periodic orbit collides with P_1 as R crosses R_2; $\delta_2 > 0$ and $\delta_4 < 0$ means that at some previous value $R^* < R_2$ two periodic orbits, one stable and one unstable, collide as R crosses R^* from above.

$(Q, B) \setminus \delta_i$	δ_2	δ_3	δ_4
$(400, 0.2)$	7×10^{-4}	-2.75×10^{-6}	15×10^{-4}
$(100, 0.4)$	48×10^{-4}	21.3×10^{-6}	6.9×10^{-4}
$(10, 0.6)$	71.6×10^{-4}	-26.45×10^{-6}	2.85×10^{-4}
$(50, 1)$	72.19×10^{-4}	-68.42×10^{-6}	3.21×10^{-4}
$(200, 1.2)$	58.98×10^{-4}	-92.14×10^{-6}	9.51×10^{-4}

Finally, in the marginal case $\delta_2 = 0$ the transition type depends entirely on the sign of δ_4. In Table 3 we show some of the values for δ_4 obtained by taking $Q = Q_c(B)$ and varying B (see Figure 5). A more detailed exploration of δ_4 as a function of B in the aforementioned way shows that, in fact, δ_4 is always positive, which then indicates that the transition is of jump type all the up to

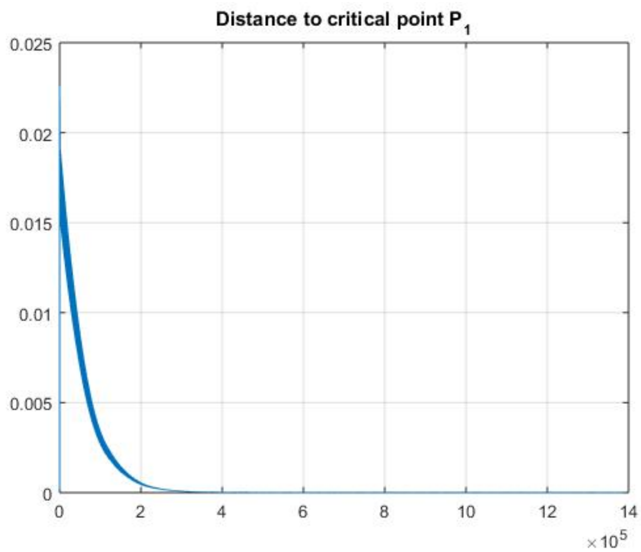

Figure 8: Distance between the trajectory and the critical point P_1 as a function of time before jump transition, shown for $Q = 200$, $B = 0.6$.

the critical curve, i.e. for all $Q \leq Q_c(B)$.

Table 3: The values of the bifurcation number δ_4 with respect to the Chandrasekhar number Q and the geometry parameter B as $\delta_2 = 0$. $\delta_4 > 0$ indicates jump transition.

$(B, Q_c(B))$	δ_4
$(0.4, 351.2605)$	0.001443
$(0.6, 321.3736)$	0.0014633
$(0.8, 349.1291)$	0.0015327
$(1, 522.6765)$	0.0013321

5. Conclusion

Our study based on the simplified model reveals that magnetic field plays an important role in determining the types of the second transition of Rayleigh-Benard convection in the presence of magnetic field. Without magnetic field, for all B in $(0, 4)$, the second transition is of jump type. If magnetic field is considered, for any fixed $B < 1.17795$, there exists a Q_c such that when $Q > Q_c$, the second transition is continuous, i.e., (25)–(28) bifurcates to a stable periodic orbit. Hence, magnetic field has a stabilizing effect in heat convection. It is also clear from the graph 5 that for large aspect ratio (roughly equal to height larger than width), under the influence of magnetic field, the second transition is continuous; whereas for small aspect ratio, the second transition is always of jump type irrespective of the magnitude of magnetic field. These conclusions, albeit drawn from the low-dimension model, may be relevant for the general Rayleigh-Benard convection under the influence of magnetic effect. In particular, it suggests the complexity of the second and the subsequent transition of the RB convection in terms of the physical parameters such as magnetic field and aspect ratio. The framework lay out in this study is still applicable for the general RB convection which will be pursued in a future work.

Acknowledgement

The work of D. Han was supported in part by ONR grant N00014-15-1-2385, by the Research Fund of Indiana University and by a seed fund of Material Research Center at Missouri University of Science and Technology; M. Hernandez was supported in part by the National Science Foundation (NSF) grant DMS-1515024, and by the Office of Naval Research (ONR) grant N00014-15-1-2662; Q. Wang was supported by the NOAA HFIP funding (Award NA16NWS4680026). The authors wish to thank Dr. Shouhong Wang for helpful discussions.

Reference

[1] L. P. Kadanoff, Turbulent heat flow: structures and scaling, Physics today 54 (8) (2001) 34–39.

[2] S. Chandrasekhar, Hydrodynamic and hydromagnetic stability, Courier Corporation, 2013.

[3] P. G. Drazin, W. H. Reid, Hydrodynamic stability, Cambridge university press, 2004.

[4] K. Kirchgässner, Bifurcation in nonlinear hydrodynamic stability, Siam Review 17 (4) (1975) 652–683.

[5] P. Rabinowitz, Existence and nonuniqueness of rectangular solutions of the bénard problem, Archive for Rational Mechanics and Analysis 29 (1) (1968) 32–57.

[6] V. Iudovich, Free convection and bifurcation, Journal of Applied Mathematics and Mechanics 31 (1) (1967) 103–114.

[7] T. Ma, S. Wang, et al., Dynamic bifurcation and stability in the rayleigh-bénard convection, Communications in Mathematical Sciences 2 (2) (2004) 159–183.

[8] T. Ma, S. Wang, Attractor bifurcation theory and its applications to rayleigh-bénard convection, Communications on Pure & Applied Analysis 2 (4) (2003) 591–599.

[9] T. Ma, S. Wang, et al., Rayleigh bénard convection: dynamics and structure in the physical space, Communications in Mathematical Sciences 5 (3) (2007) 553–574.

[10] T. Sengul, S. Wang, Pattern formation in rayleigh benard convection, arXiv preprint arXiv:1109.5655.

[11] T. Ma, S. Wang, Geometric theory of incompressible flows with applications to fluid dynamics, no. 119, American Mathematical Soc., 2005.

[12] T. Ma, S. Wang, Bifurcation theory and applications, Vol. 53, World Scientific, 2005.

[13] M. Proctor, N. Weiss, Magnetoconvection, Reports on Progress in Physics 45 (11) (1982) 1317.

[14] O. Andreev, A. Thess, C. Haberstroh, Visualization of magnetoconvection, Physics of Fluids 15 (12) (2003) 3886–3889.

[15] A. Basak, R. Raveendran, K. Kumar, Rayleigh-bénard convection with uniform vertical magnetic field, Physical Review E 90 (3) (2014) 033002.

[16] J. Dawes, Localized convection cells in the presence of a vertical magnetic field, Journal of Fluid Mechanics 570 (2007) 385–406.

[17] Q. Wang, Stability and bifurcation of a viscous incompressible plasma fluid contained between two concentric rotating cylinders, Discrete Contin. Dyn. Syst.-B 19 (2) (2014) 543 – 563.

[18] P. Pal, K. Kumar, Role of uniform horizontal magnetic field on convective flow, The European Physical Journal B 85 (6) (2012) 201.

[19] D. Yadav, R. Bhargava, G. Agrawal, Thermal instability in a nanofluid layer with a vertical magnetic field, Journal of Engineering Mathematics 80 (1) (2013) 147–164.

[20] D. Yadav, C. Kim, J. Lee, H. H. Cho, Influence of magnetic field on the onset of nanofluid convection induced by purely internal heating, Computers & Fluids 121 (2015) 26–36.

[21] D. Yadav, J. Lee, The onset of mhd nanofluid convection with hall current effect, The European Physical Journal Plus 130 (8) (2015) 162.

[22] D. Yadav, R. Mohamed, H. H. Cho, J. Lee, Effect of hall current on the onset of mhd convection in a porous medium layer saturated by a nanofluid., Journal of Applied Fluid Mechanics 9 (5).

[23] D. Yadav, J. Wang, R. Bhargava, J. Lee, H. H. Cho, Numerical investigation of the effect of magnetic field on the onset of nanofluid convection, Applied Thermal Engineering 103 (2016) 1441–1449.

[24] T. Yanagisawa, Y. Yamagishi, Y. Hamano, Y. Tasaka, K. Yano, J. Takahashi, Y. Takeda, Detailed investigation of thermal convection in a liquid

metal under a horizontal magnetic field: Suppression of oscillatory flow observed by velocity profiles, Physical Review E 82 (5) (2010) 056306.

[25] E. N. Lorenz, Deterministic nonperiodic flow, Journal of the atmospheric sciences 20 (2) (1963) 130–141.

[26] H. Gotoda, R. Takeuchi, Y. Okuno, T. Miyano, Low-dimensional dynamical system for rayleigh-benard convection subjected to magnetic field, Journal of Applied Physics 113 (12) (2013) 124902.

[27] T. Ma, S. Wang, Phase transition dynamics, Springer, 2016.

[28] H. Dijkstra, T. Sengul, J. Shen, S. Wang, Dynamic transitions of quasi-geostrophic channel flow, SIAM Journal on Applied Mathematics 75 (5) (2015) 2361–2378.

[29] C.-H. Hsia, C.-S. Lin, T. Ma, S. Wang, Tropical atmospheric circulations with humidity effects, Proc. R. Soc. A 471 (2173) (2015) 20140353.

[30] H. G. Kaper, S. Wang, M. Yari, Dynamical transitions of turing patterns, Nonlinearity 22 (3) (2009) 601.

[31] H. Liu, T. Sengul, S. Wang, Dynamic transitions for quasilinear systems and cahn-hilliard equation with onsager mobility, Journal of Mathematical Physics 53 (2) (2012) 023518.

[32] T. Sengul, J. Shen, S. Wang, Pattern formations of 2d rayleigh–bénard convection with no-slip boundary conditions for the velocity at the critical length scales, Mathematical Methods in the Applied Sciences 38 (17) (2015) 3792–3806.